# The Catalytic Power of Ketosteroid Isomerase Investigated by Computer Simulation†

Isabella Feierberg and Johan Åqvist*

*Department of Cell and Molecular Biology, Uppsala University Biomedical Center, Box 596, SE-751 24 Uppsala, Sweden*

*Received September 19, 2002; Revised Manuscript Received October 22, 2002*

ABSTRACT: Ketosteroid isomerase (KSI) catalyzes the isomerization of $\Delta^5$-3-ketosteroids and $\Delta^4$-3-ketosteroids at very high rates. Here we examine the principles underlying the catalytic efficiency of KSI by computer simulations using the empirical valence bond method in combination with molecular dynamics free energy perturbation simulations. The simulations reproduce available kinetic and structural data very well and allow us to examine several features of the catalytic mechanism in detail. It is found that about 60% of the rate enhancement is due to stabilization of the negatively charged dienolate intermediate by hydrogen bonding. The critical H-bond between Tyr16 and the intermediate is found to be a normal ionic H-bond with the preferred proton location on the tyrosine residue. The remaining 40% of the catalytic effect originates from a reduction of the reorganization energy of the reaction. The possibility of an active site water molecule occupying the empty cavity adjacent to the catalytic base (Asp40) is also addressed. The existence of such a water molecule could explain how the enzyme manages to maintain a low p$K_a$ for the general base residue.

The enzyme 3-oxo-$\Delta^5$-steroid isomerase or ketosteroid isomerase (KSI)[1] is one of the fastest enzymes that catalyze proton abstraction from nonacidic carbon atoms, i.e., keto−enol type of isomerization (*1*). Other enzymes that catalyze this kind of chemistry include, e.g., triosephosphate isomerase (*2*), citrate synthase (*3*), glyoxalase I (*4*), the enolases (*5*) (e.g., mandelate racemase, D-glucarate dehydratase, and enolase), and rubisco (*6*). Although these different enzymes are structurally unrelated, their catalytic machineries have some general features in common. That is, besides general base catalysis, all of them seem to achieve stabilization of the transient or intermediate enolate-like species through strong interactions either with cationic groups (metal ions or charged amino acid side chains) or neutral hydrogen bond donors. While the differences in substrate p$K_a$ values could perhaps explain some of the differences in the choice of catalytic groups, it is still somewhat puzzling that some of these enzymes can achieve efficient transition state stabilization by H-bonds alone (e.g., citrate synthase and KSI) when others are crucially dependent on divalent metal ions to accomplish the same task (e.g., enolases, glyoxalase I, rubisco). Of course, substrate binding may impose additional constraints in this respect. Several general proposals for how enzymes catalyzing this type of chemical steps can increase the apparent acidity of their substrates have been put forward in recent years (*5*, *7*−*11*). In addition to stabilizing the transient enolic intermediates, these enzymes also overcome high intrinsic free energy barriers associated with the corresponding nonenzymatic reactions. In KSI the lack of active site positive charges raises the question of whether the enolate can be stabilized by H-bonds alone or whether there may be other important effects involved in the enzymatic rate enhancement.

KSI participates in steroid metabolism in microorganisms and catalyzes the isomerization of $\Delta^5$-3-ketosteroids and $\Delta^4$-3-ketosteroids at an almost diffusion-controlled rate (*12*) (see Figure 1). In the initial enolization step the $\beta$-proton is abstracted from the sp$^3$-hybridized C4 carbon of the substrate, e.g., 5-androstene-3,17-dione (p$K_a$ 12.7) (*13*), situated next to the carbonyl group of the steroid A ring. The subsequent reketonization step occurs by proton transfer to the sp$^2$-hybridized C6 carbon of the formed dienolate intermediate and yields the product 4-androstene-3,17-dione (p$K_a$ 16.1) (*13*). Asp40 has been identified as the catalytic base/acid for both reaction steps (*1*). Herein, we will refer to the above-mentioned species as substrate and product, respectively.

There are to date 2 NMR and 13 X-ray structures available of wild type and mutants of KSI from *Pseudomonas putida* (*PI*) and *Pseudomonas testosteronii* (*TI*) free and in complex with different ligands including substrate, intermediate, and product analogues. For simplicity, we use the residue numbering corresponding to the *PI* sequence, and steroid atoms are numbered according to 5-androstene-3,17-dione (see Figure 1). Having 34% sequence identity, the overall fold and the active sites in all available X-ray structures as well as the kinetic properties of *PI* and *TI* are very similar. All structures show a hydrophobic active site lined with mostly nonpolar residues, and no water molecules are detected near the reaction center. The structures most relevant for this work are 4TSU (*14*) (Asp40Asn *PI* in complex with the inhibitor equilenin at 2.5 Å resolution), 1E3N (*15*) (Asp40Asn *PI* mutant complexed with equilenin at 2.0 Å

† Support from the Swedish Research Council and the National Graduate School of Scientific Computing is gratefully acknowledged.

* To whom correspondence should be addressed. Tel: 46-18-471-4109. Fax: 46-18-536971. E-mail: aqvist@xray.bmc.uu.se.

[1] Abbreviations: KSI, 3-oxo-$\Delta^5$-steroid isomerase or ketosteroid isomerase; NMR, nuclear magnetic resonance; *PI*, *Pseudomonas putida*; *TI*, *Pseudomonas testosteronii*; LBHB, low-barrier hydrogen bond; MD, molecular dynamics; FEP, free energy perturbation; EVB, empirical valence bond.

10.1021/bi026873i CCC: $22.00 
Published on Web 12/03/2002

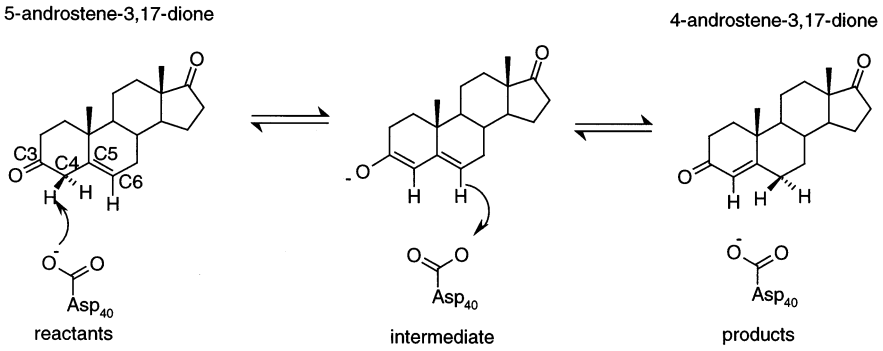


FIGURE 1: Reaction mechanism of ketosteroid isomerase. The numbering of atoms in this figure is used throughout the text.

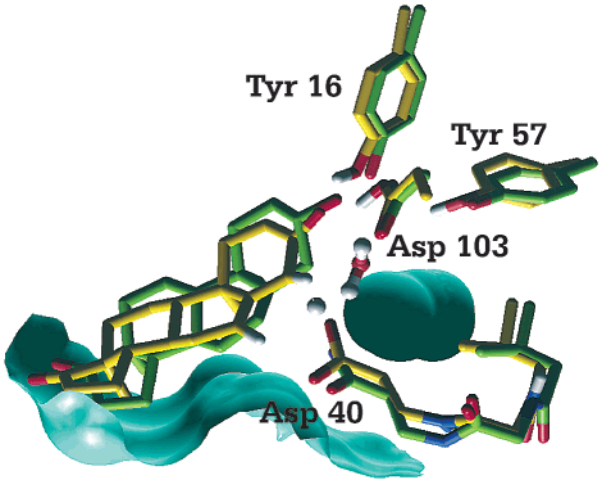


FIGURE 2: Snapshot from MD simulations of the intermediate dienolate state after proton transfer to Asp40 (yellow) superimposed on the experimental structure (*15*) of the Asp40Asn mutant of the *PI* enzyme in complex with the hydrated substrate molecule (green). Part of the outer molecular surface together with the internal cavity for the experimental structure is shown (cyan) as well as the active site water molecule Wat1 in the simulated structure.

resolution), and 1E3R (*15*) (Asp40Asn *PI* mutant complexed with the hydrated form of the substrate, 3-$\beta$-hydroxy-5-androsten-17-one at 2.5 Å resolution), since they provide information about the reactants and intermediate state geometries. The largest difference in the active site between 1E3N, 4TSU, and 1E3R is the rotation angle of the Phe56 aromatic ring located opposite the ligand on the distal side of Asp40. This indicates that the overall geometry of the active site is maintained during the initial reaction step. It can be noted that the p$K_a$ of the enol form of the intermediate is 10 (*16*) while that of the intermediate analogue equilenin is 9 (*17*), which may suggest the same protonation state of both species in complex with the enzyme. Two H-bonds donated by Asp103 and Tyr16 [p$K_a \geq 9.5$ and p$K_a = 11.6$, respectively (*1*, *18*−*20*)] to the O3 oxygen of the steroid apparently stabilize the negative charge of the dienolate intermediate (Figure 2). Mutation of either of these residues inactivates the enzyme (*18*). Tyr16 also accepts a H-bond from Tyr57, which seems to play a structural role for the correct positioning of Tyr16 (*21*). The carboxylate of Asp40 (as judged from the Asp40Asn complexes) is located next to the C4 carbon of the steroid. One of the Asp40 carboxylate oxygens is in contact with the surrounding bulk water and also accepts a H-bond from Trp120 in *PI*, while in *TI* the tryptophane is replaced by a phenylalanine. The other Asp40 oxygen, which is positioned close to C4 of the steroid, points into an empty cavity located between Tyr57, Met116, Asp40, and the ligand. This cavity is large enough to accommodate a water molecule (see Figure 2), which would satisfy H-bond possibilities of both Asp40 and Tyr57. In previous studies it has been claimed that all water is exluded from the active site in the complexed enzyme, and the possibility that a water molecule occupies this cavity has never been mentioned. In addition, no effort has been made to explain the low p$K_a$ value of Asp40 [4.75 in *TI* KSI (*22*)] in the Michaelis complex. This is particularly problematic for the *TI* enzyme, since it lacks the polar interaction with Trp120, found in the *PI* isomerase, which can stabilize its charge. In the free enzyme, the p$K_a$ of Asp40 is 4.57 (*22*), and thus the exclusion of bulk water from the active site upon binding of the hydrophobic substrate increases the p$K_a$ of Asp40 by only 0.18 units. It is thus particularly interesting to understand how the KSI active site can maintain a low p$K_a$ for Asp40, and in this work we also examine the possible energetic and structural effects of a water molecule in the cavity adjacent to Asp40. Again, it should be pointed out that earlier mechanistic discussions are largely based on the Asp40Asn structures which differ from the wild type by a negative charge.

Hitherto, a number of mechanisms for KSI have been proposed. Xue et al. initially suggested a mechanism that avoids formation of a dienolate intermediate by concerted proton abstraction and protonation of the carbonyl oxygen of the substrate carried out by Tyr16 (*23*). Such concerted acid−base catalysis was previously proposed to be a general mechanism for these types of enolization reactions (*7*). The involvement of so-called low-barrier hydrogen bonds (LBHBs) has later been put forward as a general mechanism for many enzyme-catalyzed enolization reactions (*8*, *11*). These remarkably strong H-bond interactions, which are known to exist in the gas phase, are expected to occur when the barrier in a "traditional" H-bond double-well potential decreases below the zero-point energy of the involved vibration. The proton then becomes delocalized between the heavy atoms, and the interaction is largely covalent rather than electrostatic, which makes it unusually strong. In order for an LBHB to form, the p$K_a$ values of donor and acceptor atoms should be more or less perfectly matched. For KSI, a number of mechanisms involving LBHBs have been put forward. The LBHB was first proposed to form between Tyr16 and the developing enolate (*11*, *24*), which both have a p$K_a$ value of ∼10 in solution (*16*). However, at that time the structural and mechanistic importance of Asp103 had not yet been discovered. After the discovery of this residue an alternative

mechanism, based on a solution structure of KSI in complex with a product analogue, was suggested. Here, an LBHB between Tyr16 and Asp103 was proposed to increase the strength of the ionic H-bond between Tyr16 and the steroid during the formation of the dienolate (*25*, *26*). A third alternative implied an LBHB between Tyr16 and the dienolate and a normal ionic H-bond between Asp103 and the dienolate (*14*). Finally, it has been proposed that both H-bonds donated to the dienolate by Asp103 and Tyr16 are of the normal ionic type (*1*, *27*, *28*). In the work presented here we will focus on the two latter types of mechanisms.

To assess the effect that the enzymatic environment has on the energetics of a reaction, it is necessary to compare it to its nonenzymatic counterpart. The corresponding acetate ion-catalyzed dienolate formation from substrate and product has rate constants of $6.1 \times 10^{-4}$ $s^{-1}$ and $1.3 \times 10^{-8}$ $s^{-1}$, respectively (*16*). The high activation energy is lowered by about 9 kcal/mol in the enzyme, as revealed in the free energy profile of the *TI*-catalyzed reaction (*29*). There is considerable stabilization of the intermediate dienolate state compared to the nonenzymatic acetate-catalyzed reference reaction, the first reaction step being close to thermoneutral. Since the p$K_a$ of Asp40 in the Michaelis complex is known to be 4.75, the profile shows that KSI reduces the p$K_a$ of the substrate by (maximally) 8 units to ~5. The total enzymatic barrier reduction for both deprotonation steps of substrate and product is 9 and 10 kcal/mol, respectively, while the steps involving reprotonation of the dienolate intermediate have free energy barriers that are slightly increased in the enzyme.

In this work we use molecular dynamics (MD) and free energy perturbation (FEP) simulations, in combination with an empirical valence bond (EVB) representation of the reaction potential surface, to investigate the energetics of the KSI-catalyzed reaction. With this type of methodology one can treat the entire system (enzyme, substrate, and solvent) on a micoscopic level and evaluate free energy profiles that include, e.g., solute and solvent entropic effects as well as equilibrium and nonequilibrium solvation in a realistic manner. The technique has proven to be very efficient for studying enzyme reactions in general (*30*−*35*), and in particular, it has been successful in reproducing the energetics of other enzymic keto−enol isomerization reactions (*35*−*37*).

## METHODS

Our treatment of the KSI reaction is based on the empirical valence bond formulation where a proton-transfer process can be described in terms of two (impure) VB states

$$\psi_1 = \mathrm{D{-}H\ A}$$
$$\psi_2 = \mathrm{D^-\ H{-}A^+} \qquad (1)$$

that also represent a possible mixing with a higher energy resonance form of the $D^-$ $H^+$ $A^-$ type (*30*, *31*). The effective EVB Hamiltonian in the present case involves the diagonal (diabatic) energies of the three resonance structures shown in Figure 1 and the off-diagonal terms that describe the resonance interactions between the states. Each diagonal energy function is given by

$$H_{ii} = \epsilon_i = V^{(i)}_{\mathrm{bond}} + V^{(i)}_{\mathrm{angle}} + V^{(i)}_{\mathrm{torsion}} + V^{(i)}_{\mathrm{nb,rr}} + V^{(i)}_{\mathrm{nb,rs}} + V^{(i)}_{\mathrm{ss}} + \alpha^{(i)} \qquad (2)$$

where the first three terms describe the intramolecular potential energies of the reacting fragments (here Asp40 and the steroid) by Morse bond potentials, harmonic three-atom angle bending, and proper and improper torsional angle functions. The fourth term denotes nonbonded van der Waals and electrostatic interactions within and between the reacting fragments. The fifth and the sixth terms describe the interactions between the reactants and the surrounding environment and the potential energy of the surrounding enzyme−water system, respectively. The last term of the Hamiltonian represents the intrinsic gas-phase energy of the given resonance structure with all fragments at infinite separation, i.e., noninteracting.

Combination of the EVB representation of the reaction potential surface with the MD/FEP technique allows us to drive the system between valence bond states *i* and *j* and sample system configurations along the way. At each configuration, the ground-state energy is obtained as the lowest eigenvalue of the secular equation. Besides the diagonal (diabatic) energies, the ground state also depends on the off-diagonal matrix elements, $H_{ij}$, representing the adiabatic mixing of the VB states. These off-diagonal terms as well as the gas-phase energy shifts are usually determined by fitting the EVB potential surface to available data regarding the uncatalyzed reaction profile in water (*30*, *31*, *38*) (see below).

The calculations of free energy profiles follow the FEP procedure described in ref *31*. For an elementary proton-transfer step, the two VB states are "connected" via a set of intermediate mapping potentials $\epsilon_m = \lambda_i^m \epsilon_i + \lambda_j^m \epsilon_j$, where $\epsilon_i$ is given by eq 2 and $\lambda_i^m + \lambda_j^m = 1$. The mapping vector $\vec{\lambda}_m = (\lambda_i^m, \lambda_j^m)$, defining a linear combination between the two potentials, changes between the values (1,0) of reactants and (0,1) of products. The free energy associated with changing $\epsilon_i$ to $\epsilon_j$ in *n* discrete steps is obtained as

$$\Delta G(\vec{\lambda}_n) = \Delta G(\vec{\lambda}_0 \rightarrow \vec{\lambda}_n) = -\beta^{-1} \sum_{m=1}^{n-1} \ln\langle \exp[-\beta(\epsilon_{m+1} - \epsilon_m)] \rangle_m \qquad (3)$$

where $\beta = 1/kT$ and the average $\langle\ \rangle_m$ is evaluated on the mapping potential surface $\epsilon_m$. The free energy profile $\Delta G(X)$ corresponding to trajectories moving on the actual ground-state potential, $E_g(X)$, is calculated from the umbrella sampling expression

$$\Delta G(X) = \Delta G(\vec{\lambda}_m) - \beta^{-1} \ln\langle \delta(X - X') \exp\{-\beta[E_g(X) - \epsilon_m(X)]\} \rangle_m \qquad (4)$$

where the reaction coordinate, $X = \Delta\epsilon = \epsilon_i - \epsilon_j$, is the energy gap between the two diabatic surfaces (*31*).

One advantage of the EVB method is that the gas-phase free energy difference between the two valence bond states, $\Delta\alpha_{ij} = \alpha^{(j)} - \alpha^{(i)}$, and the off-diagonal element, $H_{ij}$, describing the resonance interaction between these states, can be determined by calibrating the free energy profile of an appropriate reference reaction against experimentally

derived reaction free energies and activation barriers. In this way one can ensure that the solution free energy surface reproduces thermodynamic and kinetic data and in addition the reaction energetics of the enzyme-catalyzed reaction can be directly compared to their nonenzymatic counterpart in water. The EVB calibration procedure is described in detail elsewhere (*31*, *35*).

*Simulation Protocols.* An acetate ion (p$K_a$ 4.8) was chosen as the catalytic base in the nonenzymatic reference reaction. For the enzyme-catalyzed reaction, the X-ray structures 1E3N (*15*) and 4TSU (*14*) with the Asp40Asn mutant of *PI* complexed with equilenin were both used as starting coordinates for the simulations. The two structures are indeed very similar and yield no significant differences in the simulation results. The substrate was superimposed manually on the equilenin. All crystal waters within 18 Å from the proton abstracting carboxylate oxygen of Asp40 were kept. A water molecule, denoted Wat1, was manually placed in the empty active site cavity described above. The system was solvated with SPC water on a grid using an automated procedure in the molecular simulation program Q (*39*), which was used for all MD simulations and free energy calculations. For all reaction steps in both water and enzyme, a simulation sphere radius of 18 Å, centered on the reacting fragments, was used, with 10 kcal/mol restraints on the protein atoms situated in the outer 1.5 Å shell. The water surface was restrained according to the SCAAS model (*40*). Long-range electrostatic interactions in the $V_{ss}$ term (eq 2) outside a 10 Å cutoff distance were treated with the LRF method (*41*), while all interactions involving the reacting groups were explicitly treated.

All EVB simulations were initiated at the transition state region after slow heating to 300 K and 50 ps equilibration at this temperature. Simulations of the enzyme reaction were carried out both with and without the extra water molecule (Wat1) present. All EVB simulations used 51 discrete FEP points, and at each point 5 ps MD trajectories were calculated using a 1 fs time step and the last 3 ps at each FEP point were used for data analysis. Protein and solvent parameters were taken from the GROMOS87 force field (*42*), the Morse potentials are given in ref *35*, and the partial charges of the substrate, intermediate, and product molecules were Mulliken charges obtained from AM1 calculations. Calibration of the free energy profile of the uncatalyzed reaction was done against the available substrate and product p$K_a$s and reaction rates of the acetate-catalyzed isomerization. The free energy barriers corresponding to the rates for deprotonation of the substrate and product to form the dienolate intermediate are 19.6 and 26.0 kcal/mol, respectively, after correction with the concentration term *RT* ln 55 that arises from bringing the reacting fragments from 1 M concentration to contact distance in aqueous solution. For the calibration of the reference reaction, a constant off-diagonal element $H_{12}$ was used although it is possible to use an exponential or Gaussian function of the donor−acceptor distance as well (*31*). These alternative functional forms were tested for the initial step and gave virtually identical free energy profiles.

## RESULTS AND DISCUSSION

The calculated free energy profiles for the *PI* KSI-catalyzed reaction (with and without Wat1) are shown in Figure 3 together with the experimental free energy profile for the *TI* enzyme (*29*) and that for the uncatalyzed reaction with an acetate ion as the base (*16*). In general, both of the calculated enzyme free energy profiles are in very good agreement with the experimental results. They show that the second reaction step is rate limiting and that there is a significant stabilization of the dienolate intermediate (*29*). However, it appears that the thermodynamics of the entire reaction is best reproduced with Wat1 occupying the active site cavity. In fact, these calculations are in almost perfect agreement with the experimental data, the only difference being that the reprotonation step has a barrier that is too high by about 3 kcal/mol.

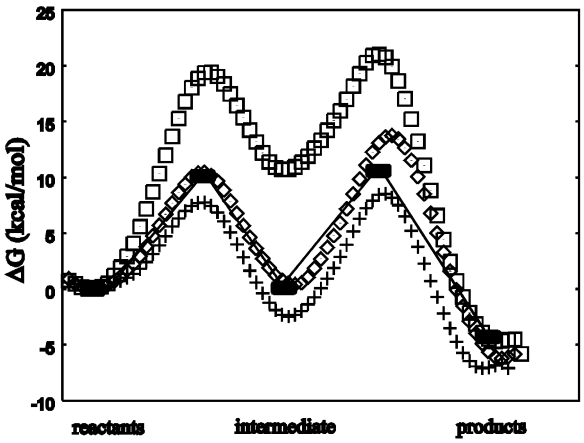


FIGURE 3: Calculated free energy profiles for the KSI-catalyzed reaction with the active site water molecule inserted (diamonds) and without the water molecule (crosses). Open squares show the simulated profile for the nonenzymatic, acetate-catalyzed reaction (*16*). Solid squares with lines show the experimental values for the *TI*-catalyzed reaction (*29*).

The simulation of the first reaction step without Wat1, on the other hand, shows an overstabilization of the intermediate by ~3 kcal/mol, and an underestimation of the barrier by the same amount, compared to the experimental results. However, the second reaction step by itself is in perfect agreement with the experimentally derived free energy profile. In fact, by shifting the whole profile of this simulation upward so that the intermediate state coincides with that of the experimental profile, the only point in disagreement is the reactant state, which is then destabilized by ~3 kcal/mol. The results of an FEP calculation, where the charge of Asp40 was gradually turned off in the reactant state with and without Wat1, showed a 7 kcal/mol relative destabilization of the aspartate in the absence of Wat1, which corresponds to a p$K_a$ increase for Asp40 by roughly 5 units. This is thus best characterized as a ground-state desolvation effect, and it seems questionable whether Asp40 would really be ionized in the Michaelis complex in the absence of the water molecule. Furthermore, the good agreement between the calculated and observed equilibrium constants for the case with Wat1 present speaks in its favor together with the fact that empty cavities adjacent to (charged) carboxylate groups in proteins are most unusual. With regard to the available crystal structures of KSI it is also noteworthy that the most relevant ones all have the Asp40Asn mutation (*14*, *15*), which may completely change the electrostatic situation in the active site.

To identify important interactions in the system that lead to enzymatic rate enhancement, it is necessary to evaluate

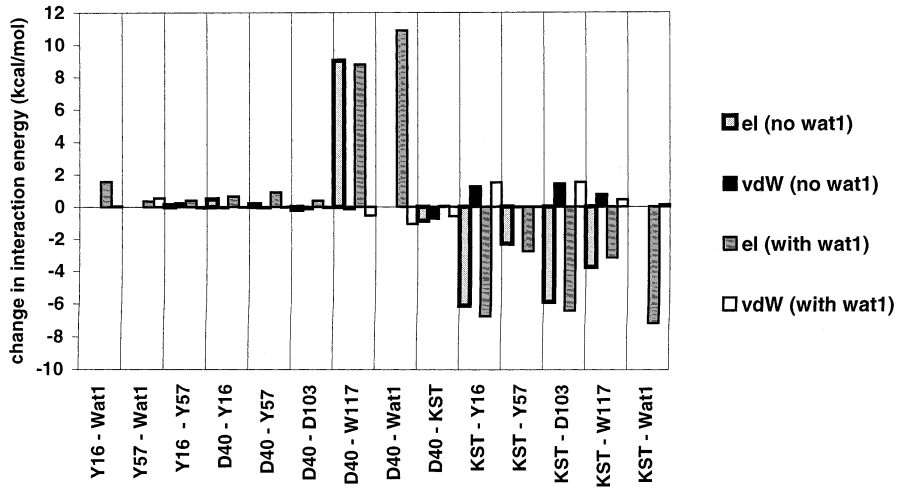


FIGURE 4: Changes in electrostatic and van der Waals interaction energies between the reacting groups and their surroundings during the first reaction step. Wat1 is the active site water molecule, and KST denotes the steroid. For each interaction four bars are shown. From left to right: the electrostatic (light gray) and van der Waals (black) energies for the simulation without Wat1 and the electrostatic (striped) and van der Waals (white) energies for the simulation with Wat1.

the calculated energetics in light of the structures obtained from the simulations. Although the H-bond pattern in the active site with Asp103 and Tyr16 donating H-bonds to the dienolate oxygen remains in all states in the simulations without Wat1, there is consistently (in several independent simulations) a change in the side chain conformation of Asp40. In the reactant and product states the negatively charged Asp40 side chain turns toward the bulk water, and the carboxylate oxygen that was pointing into the cavity now interacts with Trp120, while the other oxygen interacts with the solvent. On the other hand, the orientation of Asp40 is identical to the X-ray structures when protonated in the intermediate state, which agrees with the conclusion drawn from the FEP calculation, namely, that the Asp40 side chain can exist beside the empty cavity only when it is protonated.

In the simulation of the reactant state with Wat1, Asp40 remains directed into the cavity and interacting with the water molecule. However, the H-bond pattern involving Tyr16, Asp103, the steroid, and Wat1 differs from that in the simulation without Wat1. The substrate O3 oxygen accepts an H-bond from Tyr16, while the carboxyl hydrogen of Asp103 is directed toward Wat1, the average distance between O3 and the Asp103 hydroxyl oxygen being 3.2 Å. In the average MD structure of the intermediate state, the H-bond pattern around the dienolate oxygen is identical to that of the simulation without Wat1. In fact, the average MD structures of both simulated systems in the intermediate state are in excellent agreement with the experimentally determined geometry, where the O3 oxygen of the intermediate analogue equilenin interacts through H-bonds (distance 2.6 Å) with Tyr16 and Asp103. Tyr16 accepts a H-bond from Tyr57, which in turn accepts one from Tyr32. Figure 2 shows a representative snapshot of the active site in the intermediate state from the simulation with Wat1 superimposed on the 1E3R structure. The ligand in this structure is, in fact, the hydrated form of the substrate, which makes it the most substrate-like ligand of the available X-ray structures. In contrast to equilenin it has the C10 methyl group present, and the only difference in active site geometry between the two (simulated and experimental) structures is that the Phe56 phenyl ring is slightly rotated away from the C10 methyl in 1E3R. The solvent-accessible surface shows the position of the active site cavity in the crystal structure. Wat1 donates H-bonds to both Tyr57 and the oxygen of Asp40 that is proximal to the cavity. The binding free energy of Wat1 to the active site in the reactant state was found to be $-0.7 \pm 0.5$ kcal/mol according to a linear interaction energy calculation (*43*), which indicates that there is indeed a slight affinity for accommodating it in the cavity.

To examine the interactions of the individual active site residues with the reacting fragments in detail, the average interaction energies were monitored during the MD simulations of the reactants and intermediate states of both simulations. The results are shown in Figure 4 and demonstrate that, in the simulation without Wat1, the largest change in interaction energy in the active site is the strengthening of the Asp103−steroid and Tyr16−steroid electrostatic interactions by 6 kcal/mol each. The interaction between Asp40 and Trp117, on the other hand, weakens by 9 kcal/mol upon dienolate formation. The steroid also strengthens its electrostatic interaction with Trp117 and Tyr57 by 4 and 2 kcal/mol, respectively, when it becomes negatively charged. In the simulation with Wat1 the picture is similar. The electrostatic interactions of the steroid with Tyr16, Asp103, and Wat1 strengthen by about 7, 6, and 7 kcal/mol, respectively, while the interactions of Wat1 and Trp120 with Asp40 weaken by 11 and 9 kcal/mol, respectively.

Using the EVB method it is relatively straightforward to evaluate how much of the total barrier reduction originates from stabilization of the intermediate state. By artificially shifting the reaction free energy of the uncatalyzed reaction in solution to the calculated value in the enzyme, which is done by simply adding a negative constant to $\Delta\alpha_{ij} = \alpha^{(j)} - \alpha^{(i)}$, one can easily examine to what extent the barrier reduction is explained by just modulation of the relative p$K_a$s. The result of such a calculation for the first reaction step (including Wat1) is shown in Figure 5, where it can be seen that an excess barrier of about 4 kcal/mol still exists in the solution reaction after its equilibrium constant has (artificially) been shifted to the same value as in the enzyme. The further barrier reduction in the enzyme by that amount is thus a pure transition state stabilization that is not explained

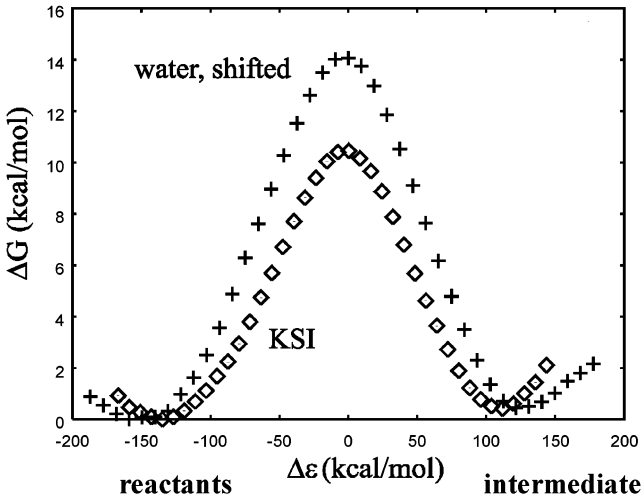


FIGURE 5: Contribution from dienolate stabilization to the total barrier reduction of the initial reaction step in KSI. Diamonds and crosses denote the enzyme-catalyzed and shifted nonenzymatic profiles, respectively. The difference in barrier height is the remainder of the enzymatic barrier reduction that is not explained by stabilization of the intermediate state. The shifted profile has been calculated from the nonenzymatic one by hypothetically changing the gas-phase energy parameter $\Delta\alpha_{ij}$ for the solution reaction so that the reaction free energy coincides with that of the enzyme-catalyzed reaction.

by stabilization of the intermediate. This effect is found to originate from the reduction of the reorganization energy of the reaction (*44*−*46*) as has been observed earlier in simulations of the related triosephosphate isomerase and glyoxalase I reactions (*35*−*37*). Overall, about 60% of the activation barrier reduction thus originates from stabilization of the intermediate while the remaining 40% is caused by lowering the reorganization energy (interestingly, this ratio is practically the same with and without Wat1 present in the active site). As has been pointed out earlier, it is the relatively rigid and preorganized nature of the enzyme active site that gives rise to the latter effect (*47*), and the reorganization energies can also be directly calculated from the diabatic free energy curves of the reaction (*36*) (for related calculations on hydride transfer reactions in dehydrogenases, see ref *34* and references cited therein). For the first reaction step of KSI the reorganization energy reduction was found to be about 20 kcal/mol (*35*). The observed stabilization of the negatively charged dienolate is, of course, also related to the preorganization of dipolar groups in the enzyme active site. Moreover, such a stabilization can be viewed as a reduction of the reorganization energy for the creation (or binding) of a negative charge rather than for transferring that charge between different groups, as in the actual chemical reaction.

It has been suggested that the transition state stabilization in the KSI-catalyzed dienolate formation step arises from an LBHB developing between Tyr16 and the dienolate (*11*, *14*, *24*) or between Asp103 and Tyr16 (*25*, *26*). Although the present results show that it is not necessary to invoke LBHBs in order to explain the catalytic efficiency of KSI, this possibility can still not be ruled out. LBHBs have indeed been detected experimentally in the gas phase, but their existence in enzymatic catalysis has been under much debate (*48*−*53*). In order for an LBHB to form, p$K_a$ matching between the donor and acceptor groups is generally said to

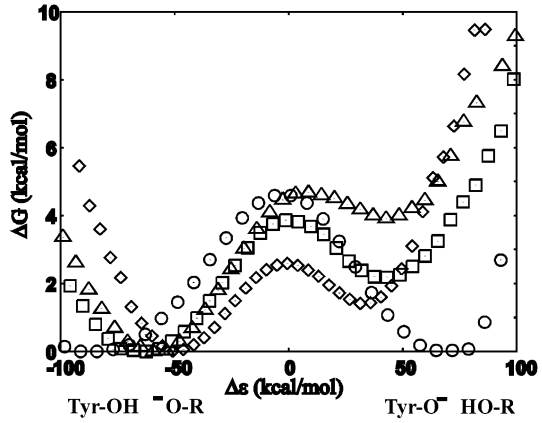


FIGURE 6: Calculated free energy profiles for the proton transfer between tyrosine (or Tyr16) and the dienolate in water (circles), vacuum (diamonds), and KSI with (squares) and without (triangles) the active site water molecule. The positive reaction free energies in the enzyme show that the preferred proton location is on the tyrosine residue.

be required. Since the charge delocalization associated with an LBHB is more favorable in a nonpolar than a polar environment, such an interaction is more probable in the gas phase or in a very hydrophobic system. Because the active site of KSI is lined by hydrophobic groups and since the p$K_a$s of the enol form of the intermediate as well as tyrosine are ∼10 in aqueous solution, it is interesting to examine the energetics of their interaction in this respect.

The above problem was addressed by EVB calculations of the free energy profile for proton transfer from Tyr16 to the dienolate, both with and without Wat1 present in the active site. The solution reaction was calibrated as usual against experimental data, where the effective barrier [including tunneling and zero-point energy effects that, however, also can be explicitly treated (see, e.g., ref *35*)] is predicted to be about 4.5 kcal/mol from accurate free energy relationships (*54*). For comparison and evaluation of the EVB model, the proton transfer was also simulated in the gas phase. In Figure 6 the free energy profile for the thermoneutral reference reaction in solution is shown together with the calculated profiles for the reaction in a vacuum and in the enzyme. The gas-phase free energy profile shows a reduced barrier of ∼2.5 kcal/mol and a slight endothermicity of 1.3 kcal/mol for the proton transfer. The strength of the H-bond in a vacuum was calculated to be about −18 kcal/mol by comparing the ground-state energy of the system at its minimum with the energy at infinite donor−acceptor distance. The mixing coefficient of the second resonance form in eq 1 corresponds to approximately 16% covalent bonding to the acceptor, and the donor−acceptor (O−O) distance is 2.49 Å. In water, on the other hand, the H-bond has a donor−acceptor distance of 2.8 Å and only 6% mixing of the second resonance form. Thus, even without any specific parametrization of this model against gas-phase data the EVB Hamiltonian reproduces the main characteristics of a strong gas-phase H-bond, or LBHB, through calibration against solution experiments. Of course, it would be possible to fit an EVB surface directly to gas-phase data or ab initio calculations, but for the present purposes this is not necessary.

Since the EVB model of the tyrosine−dienolate H-bond has the required properties both in solution and in vacuum

the effect of the enzyme environment on this interaction can be examined using the same approach. The proton transfer in KSI was examined both with and without the active site water molecule (see Figure 6), and in both cases the proton's favored location is undoubtedly on Tyr16, which means that exact p$K_a$ matching does not occur in the active site. For the enzyme profile that includes the active site water molecule the calculated endothermicity is in excellent agreement with the reported p$K_a$ shift of 1.6 p$K_a$ units = 2.2 kcal/mol for Tyr16 in KSI [this p$K_a$ has been reported as 11.6 (*24*)]. The anionic hydrogen bond is, however, strengthened in the enzyme compared to aqueous solution with the donor−acceptor distance being 2.6 Å and a 12% mixing with the covalent donor−hydrogen resonance form. Experimentally, this H-bond appears to be worth approximately 6 kcal/mol for catalysis (*18*). Like all strong H-bonds it has a significant degree of covalent character (*51*, *55*, *56*), but its strength derives mainly from electrostatic attraction (*57*). Furthermore, we note that the catalytic contribution from the H-bond is far from the 20 kcal/mol hypothesized for LBHBs. Thus, by these standards it cannot be considered to be an LBHB, according to the original definition of the concept (*9*).

A few ab initio studies of model systems related to the KSI reaction have recently been reported (*58*, *59*). In these works fairly high-level calculations have been performed on systems using a model of the substrate and two to four of the catalytic groups in the enzyme. Polarization effects of a surrounding dielectric medium were treated as in refs *58* and *59*, albeit only through single-point calculations on geometries optimized in vacuum, which would necessarily yield more gas-phase-like structures. The work by Kim et al. (*58*) addressed the reaction path of KSI but did neither give the same rate-limiting step as observed experimentally nor reproduce the activation barriers. The results of the above works were considered to support the LBHB mechanism in KSI, apparently mainly because short H-bonds (2.5−2.6 Å donor−acceptor distance) were obtained. However, in both studies the proton was clearly localized to one of the heavy atoms. The study by Pan and McAllister addressed the relative stabilities of different H-bond complexes. In that case, the most stable structure had essentially complete proton transfer from phenol (Tyr16) to butadienolate (substrate) and from formic acid (Asp103) to the phenol (*59*). This type of situation with three concerted proton transfers involved in reaching the reaction intermediate seems highly unlikely and disagrees both with crystallographic structures (*14*, *15*) and those from the present simulations, where double H-bonding (from Asp103 and Tyr16) to the dienolate is observed. As noted above, the p$K_a$ of Tyr16 is also shifted upward to 11.6 (*24*), which indeed suggests that it will remain protonated.

## CONCLUSIONS

KSI catalyzes the isomerization of $\Delta^5$-3-ketosteroids and $\Delta^4$-3-ketosteroids and is one of the fastest enzymes that catalyze proton abstraction from $sp^3$-hybridized carbon atoms adjacent to carbonyl or carboxylate groups by general base catalysis. The stabilization of the dienolate intermediate is crucial for the enzyme to attain its high turnover number. While many other enzymes that catalyze this type of reactionuse positive charges to stabilize their high-energy enolate intermediates, KSI manages to accomplish the same task by H-bonds only. Here, the catalytic power of KSI was investigated by computer simulations employing the empirical valence bond method, which allows direct comparison of the enzyme-catalyzed reaction with its nonenzymatic counterpart. This approach also includes solvation in a realistic microscopic way and involves statistical averaging over thermally accessible conformations of the system.

It appears somewhat puzzling that Asp40 has a p$K_a$ value of only 4.7 in the enzyme−substrate complex since the mostly nonpolar active site provides only one H-bond interaction for its side chain, in addition to one interaction with bulk water. However, upon inspection of X-ray structures, an empty cavity was found between Asp40, the steroid inhibitor, and Tyr57. Placing a water molecule in this cavity reduces the p$K_a$ of Asp40 by several units, and the water can interact with the carboxylate as well as Tyr16 while the overall active site structure is maintained. To investigate how it affects the reaction, all simulations of the reaction mechanism were run both with and without the water molecule inside the cavity. The calculated free energy profiles from both simulations agree reasonably well with experimental data, although in the case without the water molecule the reactant state was destabilized by ~3 kcal/mol compared to experiments. The profile with the water molecule agrees perfectly with the experimental data, except for the barrier of the second step that is overestimated by ~3 kcal/mol. From the obtained energetics and structures, it is thus not entirely clear whether the water molecule would reside in the active site during catalysis, but most of our results point in that direction. If so, a reason for it not being observed in the available crystal structures may be that the X-ray studies often have made use of the Asp40Asn mutant.

To assess which residues are important for catalysis and stabilization of the dienolate, the changes in interaction energies between the reacting fragments and the surrounding residues were monitored. They agree with the experimental result that Tyr16 and Asp103 are of major importance for the stabilization of the dienolate. On the other hand, the interactions of the reacting fragments (the steroid and Asp40) with Trp117 and the active site water molecule weaken during dienolate formation. To investigate the nature of the Tyr16−dienolate interaction, additional EVB simulations were performed of the proton transfer from the tyrosine to the intermediate. The favored proton location was found to be on Tyr16, and a p$K_a$ mismatch of about 1.6 units was obtained so that an LBHB does not seem to be formed in the active site of KSI. Furthermore, the predicted p$K_a$ difference is in excellent agreement with the known p$K_a$ values of Tyr16 and the substrate.

Finally, it was found that the relative contributions to the activation free energy reduction by KSI are about 60% from stabilization of the intermediate and about 40% from intrinsic transition state stablization caused by reduction of the reorganization energy. These two types of effects, with approximately the same ratios, have been elicited earlier in both triosephosphate isomerase and glyoxalase I (*35*−*37*), and it seems likely to us that they represent a general feature of enzyme catalyzed keto−enol isomerization reactions.

## REFERENCES


1. Pollack, R. M., Thornburg, L. D., Wu, Z. R., and Summers, M. F. (1999) *Arch. Biochem. Biophys. 370*, 9.
2. Davenport, R. C., Bash, P. A., Seaton, B. A., Karplus, M., Petsko, G. A., and Ringe, D. (1991) *Biochemistry 30*, 5821.
3. Wlassics, I. D., and Anderson, V. E. (1989) *Biochemistry 28*, 1627.
4. Vander Jagt, D. L. (1989) in *Coenzymes and Cofactors* (Dolphin, D., Poulson, R., and Avramovic, O., Eds.) p 597, John Wiley and Sons, New York.
5. Babbitt, P. C., Hasson, M. S., Wedekind, J. E., Palmer, D. R., Barrett, W. C., Reed, G. H., Rayment, I., Ringe, D., Kenyon, G. L., and Gerlt, J. A. (1996) *Biochemistry 35*, 16489.
6. Taylor, T. C., and Andersson, I. (1997) *J. Mol. Biol. 265*, 432.
7. Gerlt, J. A., and Gassman, P. G. (1992) *J. Am. Chem. Soc. 114*, 5928.
8. Gerlt, J. A., and Gassman, P. G. (1993) *Biochemistry 32*, 11943.
9. Gerlt, J. A., and Gassman, P. G. (1993) *J. Am. Chem. Soc. 115*, 11552.
10. Guthrie, J. P., and Kluger, R. (1993) *J. Am. Chem. Soc. 115*, 11569.
11. Cleland, W. W., and Kreevoy, M. M. (1994) *Science 264*, 1887.
12. Radzicka, A., and Wolfenden, R. (1995) *Science 267*, 90.
13. Pollack, R. M., Zeng, B., Mack, J. P. G., and Eldin, S. (1989) *J. Am. Chem. Soc. 111*, 6419.
14. Kim, S. W., Cha, S. S., Cho, H. S., Kim, J. S., Ha, N. C., Cho, M. J., Joo, S., Kim, K. K., Choi, K. Y., and Oh, B. H. (1997) *Biochemistry 36*, 14030.
15. Ha, N. C., Kim, M. S., Lee, W., Choi, K. Y., and Oh, B. H. (2000) *J. Biol. Chem. 275*, 41100.
16. Zeng, B., and Pollack, R. M. (1991) *J. Am. Chem. Soc. 113*, 3838.
17. Davenport, L., Knutson, J. R., and Brand, L. (1986) *Biochemistry 25*, 1186.
18. Choi, G., Ha, N. C., Kim, S. W., Kim, D. H., Park, S., Oh, B. H., and Choi, K. Y. (2000) *Biochemistry 39*, 903.
19. Kuliopulos, A., Mildvan, A. S., Shortle, D., and Talalay, P. (1989) *Biochemistry 28*, 149.
20. Thornburg, L. D., Henot, F., Bash, D. P., Hawkinson, D. C., Bartel, S. D., and Pollack, R. M. (1998) *Biochemistry 37*, 10499.
21. Kim, D. H., Jang, D. S., Nam, G. H., Choi, G., Kim, J. S., Ha, N. C., Kim, M. S., Oh, B. H., and Choi, K. Y. (2000) *Biochemistry 39*, 4581.
22. Pollack, R. M., Bantia, S., Bounds, P. L., and Koffman, B. M. (1986) *Biochemistry 25*, 1905.
23. Xue, L. A., Talalay, P., and Mildvan, A. S. (1990) *Biochemistry 29*, 7491.
24. Zhao, Q., Abeygunawardana, C., Talalay, P., and Mildvan, A. S. (1996) *Proc. Natl. Acad. Sci. U.S.A. 93*, 8220.
25. Massiah, M. A., Abeygunawardana, C., Gittis, A. G., and Mildvan, A. S. (1998) *Biochemistry 37*, 14701.
26. Zhao, Q., Abeygunawardana, C., Gittis, A. G., and Mildvan, A. S. (1997) *Biochemistry 36*, 14616.
27. Wu, Z. R., Ebrahimian, S., Zawrotny, M. E., Thornburg, L. D., Perez-Alvarado, G. C., Brothers, P., Pollack, R. M., and Summers, M. F. (1997) *Science 276*, 415.
28. Petrounia, I. P., and Pollack, R. M. (1998) *Biochemistry 37*, 700.
29. Hawkinson, D. C., Eames, T. C., and Pollack, R. M. (1991) *Biochemistry 30*, 10849.
30. Warshel, A. (1991) *Computer Modeling of Chemical Reactions in Enzymes and Solutions*, John Wiley and Sons, New York.
31. Åqvist, J., and Warshel, A. (1993) *Chem. Rev. 93*, 2523.
32. Kolmodin, K., and Åqvist, J. (1999) *FEBS Lett. 456*, 301.
33. Vagedes, P., Rabenstein, B., Åqvist, J., Marelius, J., and Knapp, E.-W. (2000) *J. Am. Chem. Soc 122*, 12254.
34. Villà, J., and Warshel, A. (2001) *J. Phys. Chem. B 105*, 7887.
35. Feierberg, I., and Åqvist, J. (2002) *Theor. Chem. Acc. 108*, 71.
36. Åqvist, J., and Fothergill, M. (1996) *J. Biol. Chem. 271*, 10010.
37. Feierberg, I., Cameron, A. D., and Åqvist, J. (1999) *FEBS Lett. 453*, 90.
38. Luzhkov, V., and Åqvist, J. (1998) *J. Am. Chem. Soc. 120*, 6131.
39. Marelius, J., Kolmodin, K., Feierberg, I., and Åqvist, J. (1998) *J. Mol. Graphics Modell. 16*, 213.
40. King, G., and Warshel, A. (1989) *J. Chem. Phys. 91*, 3647.
41. Lee, F. S., and Warshel, A. (1992) *J. Chem. Phys. 97*, 3100.
42. van Gunsteren, W. F., and Berendsen, H. J. C. (1987) *Groningen Molecular Simulation (GROMOS) Library Manual*, Biomos B.V., Nijenborgh, Groningen, The Netherlands.
43. Åqvist, J., Luzhkov, V. B., and Brandsdal, B. O. (2002) *Acc. Chem. Res. 35*, 358.
44. Warshel, A. (1978) *Proc. Natl. Acad. Sci. U.S.A. 75*, 5250.
45. Albery, W. J. (1980) *Annu. Rev. Phys. Chem. 31*, 227.
46. Cannon, W. R., and Benkovic, S. J. (1998) *J. Biol. Chem. 273*, 26257.
47. Warshel, A. (1998) *J. Biol. Chem. 273*, 27035.
48. Warshel, A., and Papazyan, A. (1996) *Proc. Natl. Acad. Sci. U.S.A. 93*, 13665.
49. Guthrie, J. P. (1996) *Chem. Biol. 3*, 163.
50. Shan, S. O., Loh, S., and Herschlag, D. (1996) *Science 272*, 97.
51. Ash, E. L., Sudmeier, J. L., De Fabo, E. C., and Bachovchin, W. W. (1997) *Science 278*, 1128.
52. Gerlt, J. A., Kreevoy, M. M., Cleland, W., and Frey, P. A. (1997) *Chem. Biol. 4*, 259.
53. Cleland, W. W. (2000) *Arch. Biochem. Biophys. 382*, 1.
54. Eigen, M. (1964) *Angew. Chem., Int. Ed. Engl. 3*, 1.
55. Cornilescu, G., Hu, J. S., and Bax, A. (1999) *J. Am. Chem. Soc. 121*, 2949.
56. Coulson, C. A., and Danielsson, U. (1954) *Ark. Fys. 8*, 239.
57. Warshel, A. (1978) *Proc. Natl. Acad. Sci. U.S.A. 75*, 2558.
58. Kim, K. S., Oh, K. S., and Lee, J. Y. (2000) *Proc. Natl. Acad. Sci. U.S.A. 97*, 6373.
59. Pan, Y., and McAllister, M. A. (2000) *THEOCHEM 504*, 29.


BI026873I